PostPrint. Marius Sandru, et al., Science, 376 (2022) 90-94
https://doi.org/10.1126/science.abj9351

An Integrated Materials Approach to Ultrapermeable and Ultraselective CO_2 Polymer Membranes

Marius Sandru,[1*] **Eugenia M. Sandru**,[1] **Wade F. Ingram**,[2] **Jing Deng**,[3] **Per M. Stenstad**,[1] **Liyuan Deng**[3] and **Richard J. Spontak**[2,4*]

[1]Department of Biotechnology & Nanomedicine, SINTEF Industry, 7034 Trondheim, Norway
[2]Department of Materials Science & Engineering, North Carolina State University, Raleigh, NC 27695, USA
[3]Department of Chemical Engineering, Norwegian University of Science & Technology, 7491 Trondheim, Norway
[4]Department of Chemical & Biomolecular Engineering, North Carolina State University, Raleigh, NC 27695, USA

ABSTRACT

Advances in membrane technologies that combine greatly improved CO_2 separation efficacy with low cost, facile fabrication, feasible upscaling, and mechanical robustness are needed to help mitigate global climate change. We introduce a hybrid integrated membrane strategy wherein a high-permeability thin film is chemically functionalized with a patchy CO_2-philic grafted-chain surface layer. A high-solubility mechanism enriches the concentration of CO_2 in the surface layer hydrated by water vapor naturally present in target gas streams, followed by fast CO_2 transport through a highly permeable (but low-selectivity) polymer substrate. Analytical methods confirm the existence of an amine surface layer. Integrated multilayer membranes prepared here are not diffusion-limited and retain much of their high CO_2 permeability while their CO_2 selectivity is concurrently increased in some cases by over ~150x.

[*] To whom correspondence should be addressed (e-mail: marius.sandru@sintef.no or rich_spontak@ncsu.edu).

An alternative to chemical absorption for the capture of CO_2 derives from polymer gas-separation membranes[6,8,9] that can be chemically tailored to achieve different levels of CO_2 selectivity and permeability. Crosslinked elastomeric membranes produced from polyethers are reverse-selective, which means that their selectivity is based on solubility rather than size (*i.e.*, diffusion) considerations, and display a strong chemical affinity for CO_2.[10-13] Glassy polymers such as polyimides and polysulfones, alternatively operate on molecular size-sieving and can be modified in various ways to alter the free-volume pathways through which penetrant molecules migrate.[14-16] In addition to these mature membrane technologies, recent studies have demonstrated that humidified block ionomers promote high CO_2 permeabilities at moderate selectivities[17,18] whereas membranes containing mobile CO_2-philic carriers can yield high CO_2 selectivities at relatively low permeabilities.[19] While these advances, as well as those regarding other classes of polymer membranes are encouraging, they confirm the trade-off between permeability and selectivity, which is manifested as the empirical Robeson upper bound.[20]

In efforts to improve the gas flux through a membrane, polymer membranes have evolved from self-standing films measuring ca. 50-100 μm thick to supported thin films typically 1-2 orders of magnitude thinner,[21,22] as illustrated in **Figure 1A**. The motivation for doing so is that thin films retain the polymer characteristics responsible for selectivity and reduce the diffusive path length (since macroporous supports afford negligible barrier to diffusion). A special case of CO_2 permeation is based on chemically-augmented facilitated transport, wherein CO_2 molecules react with specific chemical groups in a hydrated membrane and consequently permeate more quickly.[23-27] Details of these transport mechanisms are provided in the **Supplementary Material**. A polymer that is technologically promising is hydrated polyvinylamine (PVAm),[25,28] which has been reported[26] to exhibit CO_2/N_2 selectivities up to 500, depending on test conditions and specimen

preparation. Unfortunately, CO_2 permeability is diffusion-hindered even through hydrated PVAm membranes that are sub-micrometer thick. An important design paradigm drawn from this observation is that the ultrahigh CO_2 selectivity afforded by facilitated transport should be preserved, whereas the extent to which diffusive limitations negatively impact CO_2 permeability should be lessened.

One route to fabricate a polymer membrane possessing both characteristics is included in **Figure 1A**. Here, a high-solubility/fast-diffusion membrane is generated by growing an ultrathin amine-containing surface layer on a supported high-permeability polymer thin film. These hybrid integrated (HI) membranes exploit the tunable surface functionalization introduced via surface polymerization[29,30] so that their surface is covered by a highly CO_2-philic/hydrophilic nanoscale polymer layer, which is equivalent to polymer membranes for liquid separation.[31] Within this nanofabricated design (achieved using the setup pictured in **Figure S1** of the **Supplementary Material**), a mixture of CO_2, N_2 and H_2O gases initially encounters a molecularly-thin amine-rich layer (Region I in **Figure 1B**), and the CO_2 permeates through this hydrated layer due to facilitated transport without appreciable diffusive resistance. In essence, this layer serves to concentrate CO_2 before it enters the underlying substrate. An elevated population of CO_2 molecules then enters and quickly permeates through a dense polymer support (Region II) and then a macroporous support (Region III), yielding both high CO_2/N_2 selectivity and high CO_2 permeability. This scenario, depicted in **Figure 1B**, represents a combinatorial separation mechanism that marries fast facilitated transport (high CO_2 selectivity) at the membrane surface in Region I with solution-diffusion transport (high CO_2 permeability) through Region II.

Two amorphous commercialized gas-separation membranes possessing relatively high CO_2 permeability — elastomeric polydimethylsiloxane (PDMS) and glassy polytetrafluoroethylene

(PTFE AF) — have been selected here for surface modification. The PDMS membranes were procured as commercial membrane systems (DeltaMem AG, Allschwil, Switzerland) composed of PDMS thin films measuring 6 μm thick and supported on porous polyacrylonitrile mounts. The PTFE AF membranes were produced in-house by casting Teflon™ AF (amorphous fluoropolymer) 2400 (Chemours, Geneva, Switzerland) from 3M Fluorinert™ Electronic Liquid FC-72 (Nordmann Nordic AB, Stockholm, Sweden) into Teflon™ Petri dishes initially measuring 10 cm in diameter. The resultant films were first dried at 25 °C for 24 h and then vacuum-dried at 200 °C for at least 24 h to yield films measuring 25-50 μm thick. To avoid edge effects, they were cut into circles (8 cm diameter) and mechanically supported on porous poly(vinylidene fluoride) mounts (MFP2 with a pore size of 0.2 μm) manufactured by Alfa Laval (Soborg, Denmark).

The series of reactions used to chemically alter the polymer surfaces is portrayed in **Figure 1C** and begins with the introduction of initiator sites by proton extraction under UV conditions. For this purpose, benzophenone is chemically attached to each membrane surface to introduce reactive hydroxyl moieties.[32] The surface density of initiator sites was controlled by removing unbound initiator with methanol/acetonitrile and varying the initiator concentration (from 1-15% in acetonitrile), with the best CO_2 permeation results achieved at 10% benzophenone. These sites are then reacted with glycidyl methacrylate (GMA) monomer (3-15% in methanol/acetonitrile, with 10% yielding the most promising results) and polymerized under UV radiation to yield poly(glycidyl methacrylate) (PGMA) chains on the surface of each membrane. Epoxy ring-opening the PGMA chains with 20-50% ethylene diamine (EDA) in aqueous solution yielded the desired amine functionality. Additional details regarding the surface modification are provided in the **Supplementary Material**. According to X-ray photoelectron spectroscopy (XPS) spectra collected on a Kratos Ultra spectrometer (**Figure 1D**), both surface-modified polymers exhibit

evidence of surface nitrogen, confirming the presence of surface amine groups after the final reaction step. Complementary spectroscopic results are presented in **Figures S2-S4**.

Incorporation of a patchy ultrathin amine layer on the surface of PDMS, an elastomer, and PTFE AF, a glassy polymer, results in profound changes in CO_2 permeation and selectivity, as evidenced by the pressure- and temperature-dependent measurements compiled in **Figure 2**. Gas permeability tests were performed with a real-time automated data collection setup (**Figure S5**) wherein feed pressure/humidity, temperature and He sweep are precisely regulated. All the results reported here, measured from a mixed 10/90 CO_2/N_2 gas feed (at 100% relative humidity) that is representative of a broad spectrum of CO_2-related separations and a standard feed pressure (1.2 bar) and temperature (25 ± 1 °C) unless otherwise indicated, reflect the most common conditions encountered for gases containing CO_2. The dependence of CO_2 permeability on pressure displayed in **Figure 2A** confirms that the parent PDMS and PTFE AF polymer thin films possess comparable permeabilities and remain largely unaffected by increasing pressure over the range examined, as expected for solution-diffusion permeation. In contrast, the CO_2 permeabilities of the amine-functionalized membranes (am-PDMS and am-PTFE AF) are lower than their parent membranes, assuming negligible resistance from the membrane supports, and decrease with increasing pressure, which is indicative of facilitated transport.[23,25,26]

Similarly, the mixed-gas CO_2/N_2 selectivities of the unmodified and modified polymers decrease slightly with increasing pressure in **Figure 2C**, whereas the am-PDMS and am-PTFE AF polymers exhibit highly elevated selectivity levels. The temperature-dependent permeabilities provided in **Figure 2B** reveal that the parent polymers are either insensitive to or increase slightly with increasing temperature. While analogous behavior is observed for am-PTFE AF, the am-PDMS membrane appears to be more highly temperature-dependent. This response difference is

attributed to the elastomeric (flexible) nature of PDMS versus the more rigid nature of glassy PTFE AF, since the materials are expected to expand differently upon heating in accord with their coefficients of thermal expansion: 9.6×10^{-4} °C^{-1} (PDMS[33]) and 3.0×10^{-4} °C^{-1} (PTFE AF[34]). The corresponding CO_2/N_2 selectivities included in **Figure 2D** indicate that those of the parent polymers are comparably low and decrease slightly further with increasing temperature. In contrast, the selectivities of the surface-functionalized polymers are much higher but, in similar fashion as their CO_2 permeabilities, exhibit different thermal behavior. Additional measurement conditions are considered in **Figures S6-S8**.

The improvements in CO_2/N_2 selectivity apparent in **Figure 2** in the presence of moisture are a consequence of the hydrated, short-chain patchy amine layers on the surfaces of PDMS and PTFE AF. Low-voltage scanning electron microscopy (SEM) images of membranes acquired on an ultrahigh-resolution FEI Verios 460L Schottkey emitter electron microscope at an accelerating voltage of 1.0 kV before and after surface functionalization are displayed in **Figure 3**. In **Figure 3A**, the surface of the unmodified PTFE AF thin film reveals the presence of surface pits (~80-450 nm in diameter), which, upon functionalization in **Figure 3B**, become completely obscured. Since the surface of neat PDMS is featureless, **Figures 3C-D** focus on surface characteristics that develop during surface polymerization. These features resemble dewetting patterns, implying that one of the steps in the reaction sequence did not occur uniformly on the PDMS surface. Closer examination of the membranes before and after surface functionalization, however, reveals a more complex picture. Height and amplitude atomic force microscopy (AFM) images collected on an Asylum MFP-3D probe microscope are displayed for membranes based on am-PTFE AF in **Figures 3E-F** and on am-PDMS in **Figures 3G-H**. The insets correspond to the unmodified polymer films, and the height images yield root-mean-square (rms) roughness values of 6.85 and

0.99 nm for virgin PTFE AF and PDMS, respectively.

The modified surfaces consist of discrete nanodroplets confirming the likelihood of surface dewetting during functionalization. The diameters of these features measure 42-264 nm (127 nm average) on PTFE AF and 41-179 nm (95.9 nm average) on PDMS, and their mean heights vary from 97.9 nm on PTFE AF to 12.3 nm on PDMS. These nanodroplets amplify the rms surface roughness by ~10x (68.6 nm on am-PTFE AF and 8.93 nm on am-PDMS). Increases in the membrane surface area due to the presence of topological features (relative to a flat surface) are 13.2% and 3.6% for am-PTFE AF and am-PDMS, respectively, thereby providing greater opportunity for CO_2 molecules to interact with and transport through the amine-rich layer. A geometric interpretation of this increase in surface area is provided in **Figures S9** and **S10**. By changing the intensity and exposure area of the surface polymerization (as described in the **Supplementary Material**), macroscopic dewetting can be eliminated on PDMS, yielding a second-generation HI membrane designated as am-PDMS-2. According to SEM images of am-PDMS-2 membranes, no large features are evident (**Figure S11A**), whereas a nanoscale topology is discernible (**Figure S11B**). Corresponding height and phase AFM images are presented in **Figures 3I** and **3J**, respectively, (as well as 3D topographical images in **Figure S12**) and confirm the existence of a patchy nanoscale topology with a significantly reduced rms surface roughness (1.68 nm) on the am-PDMS-2 membranes. The circled features in **Figures 3I-J** identify protrusions measuring up to ~12 nm in height that are soft relative to the surrounding matrix, indicating that they represent low-density, surface-grafted chain patches. Avoiding surface heterogeneities on the functionalized PDMS membranes not only increases uniformity but also improves both CO_2 permeability (**Figure 2B**) and CO_2/N_2 selectivity (**Figure 2C**).

The performance of the present HI membranes relative to other polymer membranes intended

for CO_2 separation is routinely assessed on a Robeson plot, which evaluates membrane selectivity as a function of permeability. This representation identifies the empirical upper bound that reflects the trade-off between selectivity and permeability. As membranes have continued to improve since the original upper bound was identified,[35] the position of the upper bound has progressively shifted upward. The upper bound identified by Robeson[20] is identified in **Figure 4A**, which compares membranes that function according to the solution-diffusion mechanism. Included in this figure is a more recent (and shifted) upper bound proposed by Comesaña-Gándara *et al*.[36] in 2019 on the basis of polymers of intrinsic microporosity (PIMs). The PIM membranes afford very high CO_2 permeabilities at modest CO_2/N_2 selectivity levels,[37,38] whereas a variety of other membranes also displayed in **Figure 4A** range in permeability and selectivity from relatively low to relatively high at ~25-35 °C. To provide an additional classification description of these performance metrics, we divide the Robeson plot into quadrants and refer to membranes exhibiting CO_2 permeabilities in excess of 10^3 Barrer [1 Barrer = 10^{-10} cm^3 (STP)-cm/(cm^2-s-cm Hg)] as ultrapermeable (uP) and membranes achieving CO_2/N_2 selectivities greater than 10^2 as ultraselective (uS). While many of the membranes presented in **Figure 4A** (including those prepared from unmodified PTFE AF and PDMS) are uP in the 4th quadrant, surprisingly few are uS. In fact, two types of membranes evaluated for pilot-scale separation of CO_2 from flue gas are neither uP nor uS (in the 3rd quadrant). This disparity suggests that membranes fabricated for CO_2 capture focus primarily on improved permeability.[12,36,39]

Examples satisfying the criterion set forth above for uS membranes in the 2nd quadrant of **Figure 4A** are cellulose nanofiber/ionic liquid (CNF/IL) membranes (which rely on hydrated IL nanochannels),[19] as well as most of the am-PDMS and am-PDMS-2 HI membranes investigated here and several materials reported in the literature. Only a few membranes including a bioinspired

thin film[40] and several membranes incorporating graphene oxide nanosheets[41-43] can, however, be classified as both uP and uS in the 1st quadrant of **Figure 4A**. In marked contrast, all the am-PTFE AF membranes investigated here at temperatures from 25 to 55 °C, as well as the am-PDMS-2 membrane evaluated at 55 °C, are both uP and uS. Although surface amination of the PTFE AF membranes reduces their CO_2 permeability by 50-60%, the corresponding increase in CO_2/N_2 selectivity is ~150x greater. These results confirm that the patchy, low-density surface amine layer provides a highly hydrophilic and CO_2-philic environment that absorbs and transports CO_2 molecules via facilitated transport while the highly permeable substrate provides contiguous pathways with little barrier to molecular diffusion. For added comparison, the results displayed in **Figure 4B** confirm that the transport metrics reported here for the HI membranes possess higher CO_2 selectivities than most purely facilitated-transport membranes, which predominantly lie in the 2nd quadrant (along with two selected for pilot-scale evaluation).

In **Figure 4A**, the CO_2/N_2 selectivity achieved at 1,200 Barrer for the am-PTFE AF membrane is substantially higher than the Robeson[20] or PIM-based[36] upper-bound thresholds (by ~30x and ~20x, respectively). Equally important is our observation that the enhanced separation performance of am-PTFE AF at different temperatures in **Figure 4A** appears more consistent compared to that achieved with the am-PDMS membranes. The CO_2 transport characteristics of the am-PTFE AF and am-PDMS-2 membranes converge as the amine surface layers exhibit less heterogeneities during polymerization (detailed in the **Supplementary Material**). Differences in separation performance accompanying variations in surface modification are considered in **Figures S13-S15**, and the results reported here for CO_2/N_2 gas mixtures are extended to CO_2/CH_4 mixtures in **Figure S16**, which reveals that the am-PTFE AF membranes retain their uP and uS performance with regard to CO_2 in the case of two dissimilar gas mixtures. In addition, aspects of

durability and adaptability of the am-PDMS-2 and am-PTFE AF membranes are examined in **Figures S17** and **S18**, respectively, and results collected from single- and mixed-gas tests are quantitatively compared in **Figure S19** to further elucidate the molecular-level mechanism by which CO_2 permeates through the present HI membranes.

While the results reported herein are highly encouraging, three other relevant issues should be recognized. First, the membranes developed here derive from polymers that are already used for commercial gas separations, in which case they are widely available and the processes required to manufacture and upscale gas-separation modules for industrial operations would accommodate the surface-functionalized analogs. Second, since the PTFE AF and PDMS membranes are already in commercial use, the added expense of surface functionalization is most likely much less than introducing a new designer membrane. Third, the methodology described in this study is not restricted to PTFE AF and PDMS with a patchy, amine-rich surface layer. We have selected the systems discussed here as exemplars to provide proof of concept. By marrying the facilitated transport of a molecularly thin amine surface layer with a high-permeability polymer thin film, we have successfully demonstrated that HI membranes can be nanofabricated to take advantage of this high-solubility/quick-diffusion combination and produce next-generation membranes that, instead of being limited by a permeability-selectivity trade-off, are both uP and uS.

References

1. V. Masson-Delmotte *et al.*, "Global warming of 1.5 °C," *An IPCC Special Report on the Impacts of Global Warming of 1.5 °C above Pre-Industrial Levels and Related Global Greenhouse Gas Emission Pathways, in the Context of Strengthening the Global Response to the Threat of Climate Change, Sustainable Development, and Efforts to Eradicate Poverty* (World Meteorological Organization, Geneva, Switzerland, 2018).

2. M. Meinshausen, N. Meinshausen, W. Hare, S. C. B. Raper, K. Frieler, R. Knutti, D. J. Frame, M. R. Allen, Greenhouse-gas emission targets for limiting global warming to 2 °C. *Nature* **458**, 1158-1162 (2009).

3. O. Edenhofer, R. Pichs-Madruga, Y. Sokona, J. C. Minx, E. Farahani, S. Kadner, K. Seyboth, P. Eickemeir, B. Kriemann, J. Savolainen, S. Schlömer, C. V. Stechow, T. Zwickel, "Mitigation of climate change," *Contribution of Working Group III to the Fifth Assessment Report of the Intergovernmental Panel on Climate Change* (World Meteorological Organization, Geneva, Switzerland, 2014).

4. https://research.noaa.gov/article/ArtMID/587/ArticleID/2764/Coronavirus-response-barely-slows-rising-carbon-dioxide (reported June 7, 2021).

5. M. Bui, C. S. Adjiman, A. Bardow, E. J. Anthony, A. Boston, S. Brown, P. S. Fennell, S/ Fuss, A. Galindo, L. A. Hackett, J. P. Hallett, H. J. Herzog, G. Jackson, J. Kemper, S. Krevor, G. C. Maitland, M. Matuszewski, I. S. Metcalfe, C. Petit, G. Puxty, J. Reimer, D. M. Reiner, E. S. Rubin, S. A. Scott, N. Shah, B. Smit, J. P. M. Trusler, P. Webley, J. Wilcox, N. M. Dowell, Carbon capture and storage (CCS): the way forward. *Energ. Environ. Sci.* **11**, 1062-1176 (2018).

6. M. E. Boot-Handford, J. C. Abanades, E. J. Anthony, M. J. Blunt, S. Brandani, N. M. Dowell, J. R. Fernández, M. Ferrari, R. Gross, J. P. Hallett, R. S. Haszeldine, P. Heptonstall, A. Lyngfelt, Z. Makuch, E. Mangano, R. T. J. Porter, M. Pourkashanian, G. T. Rochelle, N. Shah, J. G. Yao, P. S. Fennell, Carbon capture and storage update. *Energ. Environ. Sci.* **7**, 130-189 (2014).

7. G. T. Rochelle, Amine scrubbing for CO_2 capture. *Science* **325**, 1652-1654 (2009).

8. D. S. Sholl, R. P. Lively, Seven chemical separations to change the world. *Nature News* **532**, 435 (2016).

9. J. M. S. Henis, M. K. Tripodi, The developing technology of gas separating membranes. *Science* **220**, 11-17 (1983).

10. N. P. Patel, A. C. Miller, R. J. Spontak, Highly CO_2-permeable and selective polymer nanocomposite membranes. *Adv. Mater.* **15**, 729-733 (2003).

11. H. Lin, E. Van Wagner, B. D. Freeman, L. G. Toy, R. P. Gupta, Plasticization-enhanced hydrogen purification using polymeric membranes. *Science* **311**, 639-642 (2006).

12. S. Wang, X. Li, H. Wu, Z. Tian, Q. Xin, G. He, D. Peng, S. Chen, Y. Yin, Z. Jiang, M. D. Guiver, Advances in high permeability polymer-based membrane materials for CO_2 separations. *Energ. Environ. Sci.* **9**, 1863-1890 (2016).

13. J. Liu, S. Zhang, D. Jiang, C. M. Doherty, A. J. Hill, C. Cheng, H. B. Park, H. Lin, Highly polar but amorphous polymers with robust membrane CO_2/N_2 separation performance. *Joule* **3**, 1881-1894 (2019).

14. M. D. Guiver, Y. M. Lee, Polymer rigidity improves microporous membranes. *Science* **339**, 284-285 (2013).

15. L. M. Robeson, Z. P. Smith, B. D. Freeman, D. R. Paul, Contributions of diffusion and solubility selectivity to the upper bound analysis for glassy gas separation membranes. *J. Membr. Sci.* **453**, 71-83 (2014).

16. M. Galizia, W. S. Chi, Z. P. Smith, T. C. Merkel, R. W. Baker, B. D. Freeman, Polymers and mixed matrix membranes for gas and vapor separation: A review and prospective opportunities. *Macromolecules* **50**, 7809-7843 (2017).

17. Z. Dai, L. Ansaloni, J. J. Ryan, R. J. Spontak, L. Deng, Nafion/IL hybrid membranes with tuned nanostructure for enhanced CO_2 separation: effects of ionic liquid and water vapor. *Green Chem.* **20**, 1391-1404 (2018).

18. Z. Dai, J. Deng, H. Aboukeila, J. Yan. L, Ansaloni, K. P. Mineart, M. Giacinti Baschetti, R. J. Spontak, L. Deng, Highly CO_2-permeable membranes derived from a midblock-sulfonated multiblock polymer after submersion in water. *NPG Asia Mater.* **11**, 53 (2019).

19. S. Janakiram, L. Ansaloni, S. Jin, X. Yu, Z. Dai, R. J. Spontak, L. Deng, Humidity-responsive molecular gate-opening mechanism for gas separation in ultraselective nanocellulose/IL hybrid membranes. *Green Chem.* **22**, 3546-3557 (2020).

20. L. M. Robeson, The upper bound revisited. *J. Membr. Sci.* **320**, 390-400 (2008).

21. R. W. Baker, B. T. Low, Gas separation membrane materials: A perspective. *Macromolecules* **47**, 6999-7013 (2014).

22. H. B. Park, J. Kamcev, L. M. Robeson, M. Elimelech, B. D. Freeman, Maximizing the right stuff: The trade-off between membrane permeability and selectivity. *Science* **356**, eaab0530 (2017).

23. R. D. Noble, Analysis of facilitated transport with fixed site carrier membranes. *J. Membr. Sci.* **50**, 207-214 (1990).

24. W. J. Koros, R. Mahajan, Pushing the limits on possibilities for large scale gas separation: Which strategies? *J. Membr. Sci*. **175**, 181-196 (2000).

25. L. Deng, T.-J. Kim, M.-B. Hägg, Facilitated transport of CO_2 in novel PVAm/PVA blend membrane. *J. Membr. Sci.* **340**, 154-163 (2009).

26. M. Sandru, S. H. Haukebø, M.-B. Hägg, Composite hollow fiber membranes for CO_2 capture. *J. Membr. Sci.* **346**, 172-186 (2010).

27. J. Liao, Z. Wang, C. Gao, S. Li, Z. Qiao, M. Wang, S. Zhao, X. Xie, J. Wang, S. Wang, Fabrication of high-performance facilitated transport membranes for CO_2 separation. *Chem. Sci.* **5**, 2843-2849 (2014).

28. B. Wang, Z. Qiao, J. Xu, J. Wang, X. Liu, S. Zhao, Z. Wang, M. D. Guiver, Unobstructed ultrathin gas transport channels in composite membranes by interfacial self-assembly. *Adv. Mater.* **32**, 1907701 (2020).

29. S. Edmondson, V. L. Osborne, W. T. S. Huck, Polymer brushes via surface-initiated polymerizations. *Chem. Soc. Rev*. **33**, 14-22 (2004).

30. M. A. C. Stuart, W. T. S. Huck, J. Genzer, M. Müller, C. Ober, M. Stamm, G. B. Sukhorukov, I. Szleifer, V. V. Tsukruk, M. Urban, F. Winnik, S. Zauscher, I. Luzinov, S. Minko, Emerging applications of stimuli-responsive polymer materials. *Nat. Mater*. **9**, 101-113 (2010).

31. J. R. Werber, C. O. Osuji, M. Elimelech, Materials for next-generation desalination and water purification membranes. *Nat. Rev. Mater.* **1**, 16018 (2016).

32. J. Deng, L. Wang, L. Liu, W. Yang, Developments and new applications of UV-induced surface graft polymerizations. *Prog. Polym. Sci.* **34**, 156-193 (2009).

33. B. E. Schubert, D. Floreano, Electronic Supplementary Information (ESI): Variable stiffness material based on rigid low-melting-point-alloy-microstructures embedded in soft poly(dimethylsiloxane) (PDMS). *RSC Adv.* **3**, 24671-24679 (2013).

34. https://www.teflon.com/en/-/media/files/teflon/teflon-af-solutions-product-info.pdf

35. L. M. Robeson, Correlation of separation factor versus permeability for polymeric membranes. *J. Membr. Sci.* **62**, 165-185 (1991).

36. B. Comesaña-Gándara, J. Chen, C. G. Bezzu, M. Carta, I. Rose, M. Ferrari, E. Esposito, A. Fuoco, J. C. Jansen, N. B. Mckeown, Redefining the Robeson upper bounds for CO_2/CH_4 and CO_2/N_2 separations using a series of ultrapermeable benzotriptycene-based polymers of intrinsic microporosity. *Energ. Environ. Sci.* **12**, 2733-2740 (2019).

37. Z.-X. Low, P. M. Budd, N. B. McKeown, D. A. Patterson, Gas permeation properties, physical aging, and its mitigation in high free volume glassy polymers. *Chem. Rev.* **118**, 5871-5911 (2018).

38. A. A. Shamsabadi, M. Rezakazemi, F. Seidi, H. Riazi, T. Aminabhavi, M. Soroush, Next generation polymers of intrinsic microporosity with tunable moieties for ultrahigh permeation and precise molecular CO_2 separation. *Prog. Energ. Combust. Sci.* **84**, 100903 (2021).

39. W. J. Koros, C. Zhang, Materials for next-generation molecularly selective synthetic membranes. *Nat. Mater.* **16**, 289-297 (2017).

40. Z. Wang, Y. Zhang, J. Wang, Y. Zhang, Bioinspired porous organic polymer-functionalized membranes for efficient CO_2 capture. *Sustain. Energ. Fuels* **4**, 1191-1198 (2020).

41. Q. Xin, Z. Li, C. Li, S. Wang, Z. Jiang, H. Wu, Y. Zhang, J. Yang, X. Cao, Enhancing the CO_2 separation performance of composite membranes by the incorporation of amino acid-functionalized graphene oxide. *J. Mater. Chem. A* **3**, 6629-6641 (2015).

42. X. Li, Y. Cheng, H. Zhang, S. Wang, Z. Jiang, R. Guo, H. Wu, Efficient CO_2 capture by functionalized graphene oxide nanosheets as fillers to fabricate multi-permselective mixed matrix membranes. *ACS Appl. Mater. Interfaces* **7**, 5528-5537 (2015).

43. M. Chen, F. Soyekwo, Q. Zhang, C. Hu, A. Zhu, Q. Liu, Graphene oxide nanosheets to improve permeability and selectivity of PIM-1 membrane for carbon dioxide separation. *J. Ind. Eng. Chem*. **63**, 296-302 (2018).

44. S. I. Voicu, M. Sandru, Composite hybrid membrane materials for artificial organs, in *Handbook of Bioceramics and Biocomposites* (I. V. Antoniac, Ed.), Springer: Cham, Switzerland, 2016, pp. 407-429.

45. M. C. Annesini, L. Marrelli, V. Piemonte, L. Turchetti, Blood oxygenators and artificial lungs, in *Artificial Organ Engineering*. Springer London: London, 2017, pp. 117-161.

46. N. Naito, K. Cook, Y. Toyoda, N. Shigemura, Artificial lungs for lung failure: JACC technology corner. *J. Am. Coll. Cardiol.* **72**, 1640-1652 (2018).

47. J. Knox, Development of carbon dioxide removal systems for NASA's deep space human exploration missions 2017-2018, in *Proc., 48th Int. Conf. Environ. Syst.* Albuquerque, New Mexico, 2017.

48. R. Hanna, A. Abdulla, Y. Xu, D. G. Victor, Emergency deployment of direct air capture as a response to the climate crisis. *Nat. Commun*. **12**, 368 (2021).

Acknowledgments

This study was supported by the Research Council of Norway through the POLYMEM project (Grant No. 254791) in the CLIMIT program and UEFSCDI Romania through the CO2Hybrid project (Grant No. 13/2020), and we thank the SINTEF Industry personnel involved in membrane fabrication, characterization and testing, especially Mr. L. E. Parnas, Mr. Ø. Dahl and Dr. M. T. Guzmán-Gutiérrez. Work performed at NC State used instrumentation maintained in the NC State Analytical Instrumentation Facility (AIF), supported by the State of North Carolina, and the Duke University Shared Materials Instrumentation Facility (SMIF). Both AIF and SMIF are members of the North Carolina Research Triangle Nanotechnology Network (RTNN), which is supported by the National Science Foundation (award number ECCS-2025064) as part of the National Nanotechnology Coordinated Infrastructure (NNCI). We are grateful to Mr. C. B. Mooney at NC State for assistance with the microscopy analyses.

PostPrint. Marius Sandru, et al., Science, 376 (2022) 90-94
https://doi.org/10.1126/science.abj9351

Figures with captions

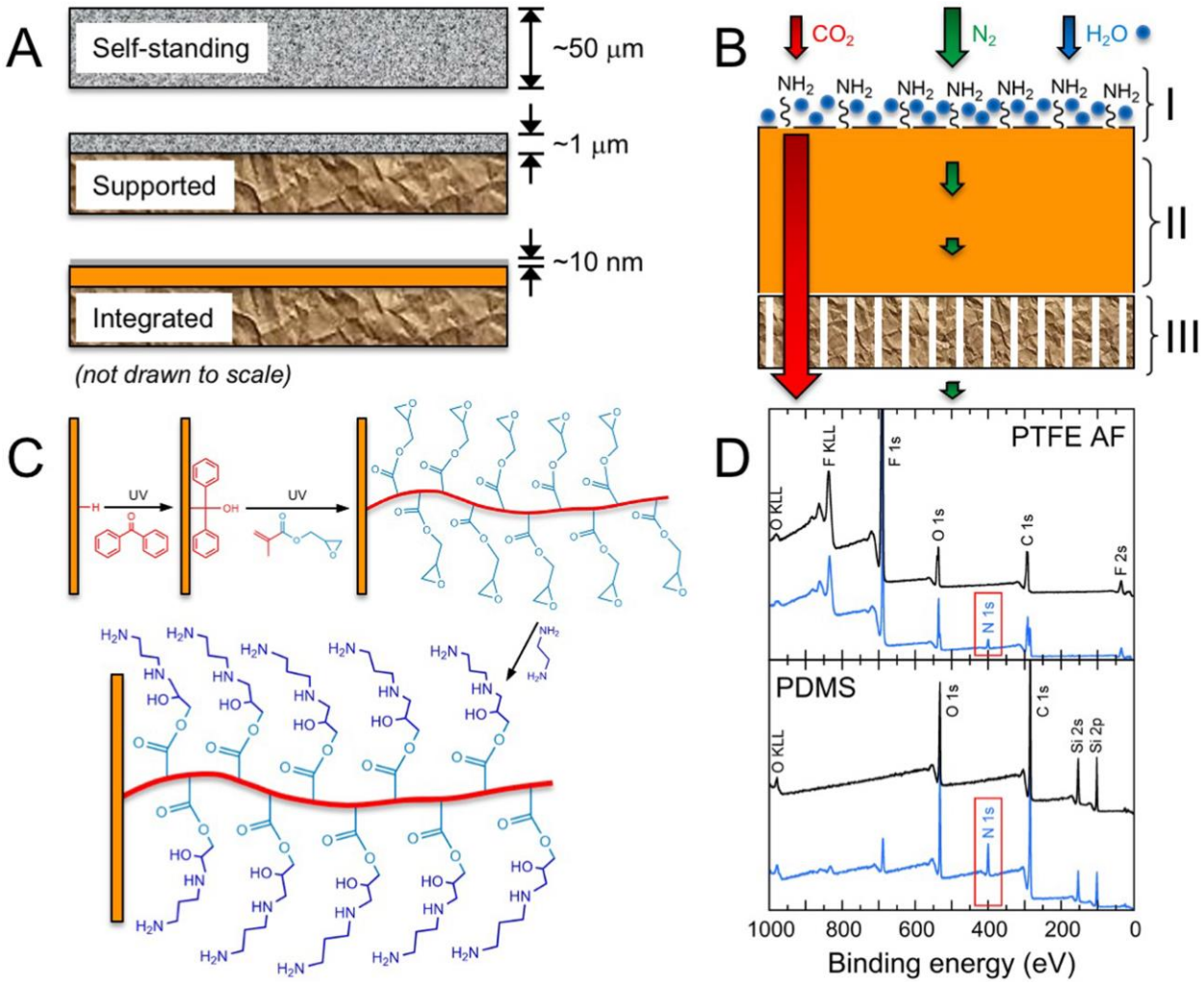

Figure 1. (A) Schematic diagram displaying the evolution of gas-separation polymer membranes from self-standing to supported to integrated (labeled). (B) Illustration of the underlying concept behind the present hybrid integrated (HI) membranes. Here, a surface-grown amine-rich layer (Region I) is grown on the surface of a highly permeable polymer thin film (Region II) supported by conventional macroporous polymers (Region III). Selectivity is exclusively achieved in Region I, which requires hydration. (C) The chemical route employed to grow amine-modified chains on polymer substrates. See the text and **Supplementary Material** for details. (D) Representative XPS spectra acquired from PTFE AF (top) and PDMS (bottom) membranes before (black lines) and after (blue lines) surface modification. The presence of the N1s peak associated with the amine-rich surface layer is highlighted in each surface-modified spectrum.

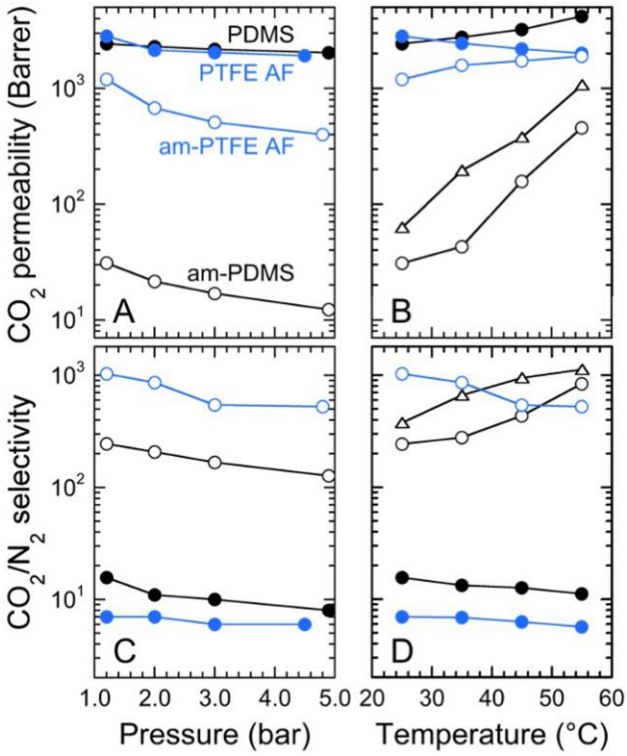

Figure 2. (A,B) CO_2 permeability and (C,D) CO_2/N_2 selectivity values measured as functions of (A,C) feed pressure and (B,D) temperature from mixed gases for membranes derived from PDMS (black lines) and PTFE AF (blue lines) before and after surface modification (labeled in A). Included in (C) are measurements from am-PDMS-2 membranes (△). The solid lines serve to connect the data. In variable-pressure tests, the temperature is maintained at 25 ± 1 °C, whereas the pressure in variable-temperature tests is kept at 1.2 bar and the feed stream is fully humidified (100% relative humidity).

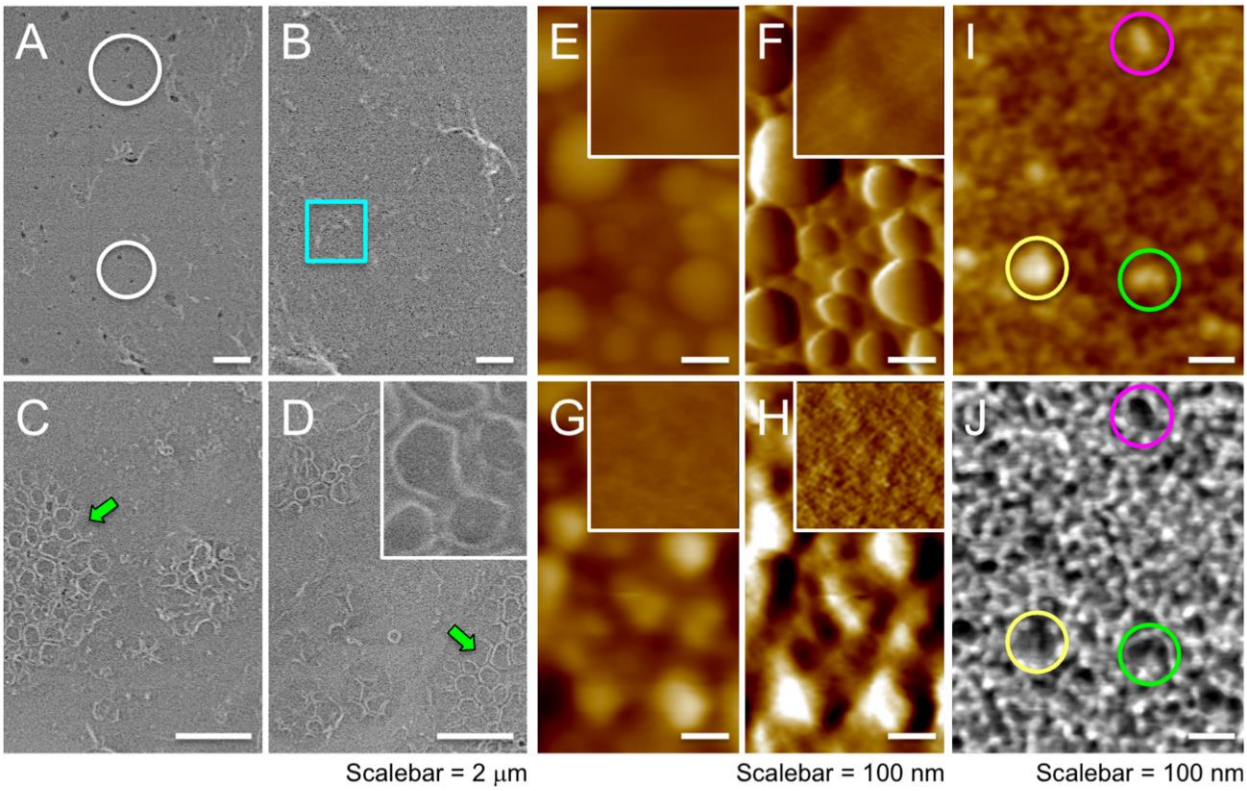

Figure 3. Low-voltage planar SEM images of solvent-cast PTFE AF membranes (A) before and (B) after surface modification. Examples of pits measuring between *ca*. 80 and 450 nm in diameter are highlighted by circles in (A), whereas a region that is reminiscent of ridges such as those evident in (A) is identified by the square in (B). The SEM images in (C,D) reveal the surface features that develop on first-generation PDMS membranes upon surface modification. The inset in (D) is a 3x enlargement of one of the regions identified by arrows. Complementary AFM (E,G) height and (F,H) amplitude images correspond to (E,F) PTFE AF and (G,H) PMDS membranes after surface modification (the inset displayed at the same magnification in each frame is acquired from the parent, unmodified surface). The paired height and phase AFM images of the surface of an am-PDMS-2 membrane in (I) and (J), respectively, confirm the existence of patchy amine-rich regions. The color-matched circles identify protrusions (light) in (I) that are mechanically soft (dark) in (J). Values of the surface rms roughness measured from AFM images such as these are provided in the text, and 3D topographical images of the am-PDMS-2 membrane are included in **Figure S12**.

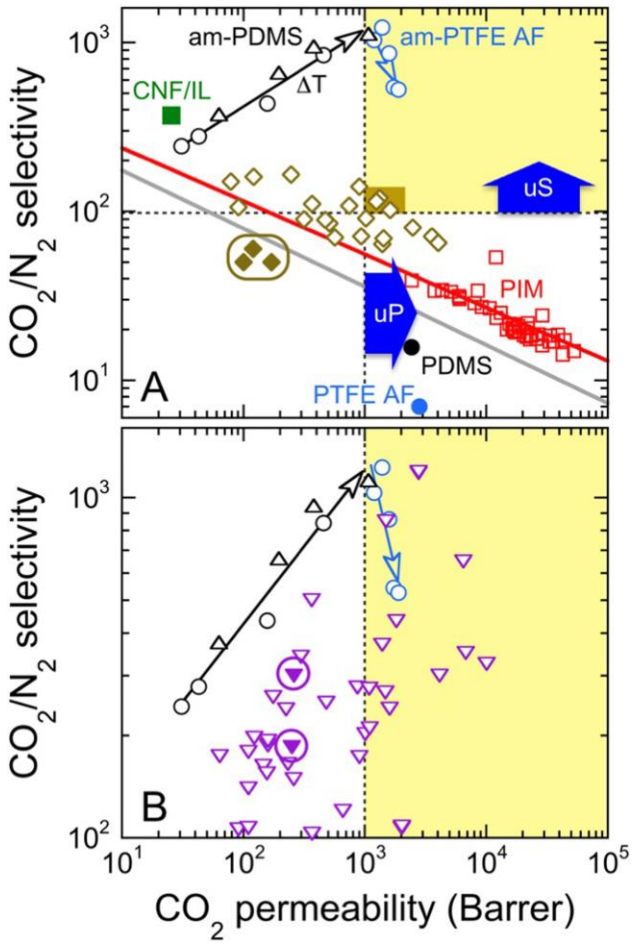

Figure 4. In (A), performance metrics of the present HI membranes (am-PDMS, ○; am-PDMS-2, △; am-PTFE AF, ○) relative to their parent materials (PDMS, ●; PTFE AF, ●), as well as other polymer membranes proposed for CO_2 capture on the basis of the SD mechanism. According to the requirements proposed here, ultrapermeable (uP) membranes exhibiting CO_2 permeabilities beyond 10^3 Barrer (in the 4th quadrant) include both PDMS and PTFE AF precursors, in addition to several other promising polymers (◇) and those in the polymer of intrinsic microporosity (PIM, □) category. Membranes subjected to pilot-scale evaluation (◆) are identified in the 3rd quadrant and listed in **Table S1**. In the 2nd quadrant, ultraselective (uS) membranes such as those based on IL-containing CNF[19] (■) reach CO_2/N_2 selectivities over 10^2 at lower CO_2 permeability levels. The Goldilocks (1st) quadrant (shaded yellow) combines both uP and uS performance. The solid lines identify the permeability-selectivity tradeoff proposed by Robeson[20] for various polymer membranes (gray) and more recently by Comesaña-Gándara *et al.*[36] for PIM membranes (red). In (B), performance metrics of the HI membranes relative to hydrated FT membranes (▽) in the 1st and 2nd quadrants only. Promising membranes assessed in pilot-scale testing (▼) are circled and compiled in **Table S1**. The color-coded arrows in (A) and (B) indicate the effect of increasing temperature (ΔT) on the HI membranes derived from PDMS and PTFE AF.